Hutnické listy č. 4-6/2024, roč. LXXVII
ISSN 0018-8069

Influence of temperature and working rolls rotational speed of the rolling mill on the qualitative properties of seamless N80 steel tubes

Vliv teploty a rychlosti otáčení pracovních válců děrovací stolice na kvalitativní vlastnosti bezešvých trubek z oceli N80

doc. Ing. Petr Jonšta, Ph.D.[1,2]; **Ing. Jan Kander** [1,2]; **Ing. Roman Noga** [1]

[1] MATERIÁLOVÝ A METALURGICKÝ VÝZKUM s.r.o., Pohraniční 693/31, Vítkovice, 703 00 Ostrava, Česká republika

[2] Vysoká škola báňská – Technická univerzita Ostrava, Fakulta materiálově-technologická, Katedra materiálového inženýrství a recyklace, 17. listopadu 2172/15, 708 00 Ostrava-Poruba, Česká republika

The formability of seamless tube production, specifically the initial step of the Mannesmann process—referred to as punching—was investigated through laboratory physical modeling using a "Universal Rolling Mill" at MATERIAL & METALLURGICAL RESEARCH Ltd. The material studied was a medium-carbon V-Ti-N microalloyed N80 steel. The experiments were conducted at four different heating temperatures and at varying rotational speeds of the working rolls, with all other rolling mill parameters kept constant. In terms of deformation parameters, the most pronounced necking of the punched sample, particularly at both ends, was observed with an increase in temperature and strain rate. The applied torque exhibited a decrease with rising temperature and lower working roll speeds. Additionally, both the punching duration and total electrical power consumption showed a reduction as temperature increased and deformation rate was elevated.

***Key words**: Laboratory physical modelling, punching, seamless tubes, N80 carbon steel, temperature, working rolls rpm*

Tvařitelnost bezešvých trubek, konkrétně počáteční krok Mannesmannova procesu – děrování – byla zkoumána laboratorním fyzikálním modelování pomocí „univerzální válcovací stolice“ ve společnosti MATERIÁLOVÝ & METALURGICKÝ VÝZKUM, s.r.o. Studovaným materiálem byla středně uhlíková V-Ti-N mikrolegovaná ocel N80. Experimenty byly prováděny při čtyřech různých teplotách ohřevu a při různých rychlostech otáčení pracovních válců, přičemž všechny ostatní parametry válcovací stolice byly udržovány konstantní. Z hlediska deformačních parametrů bylo pozorováno nejvýraznější úžení vyděrovaného vzorku, zejména na obou koncích, se zvýšením teploty a rychlosti deformace. Aplikovaný kroutící moment vykazoval pokles s rostoucí teplotou a nižšími rychlostmi otáčení pracovních válců. Doba děrování a rovněž celková spotřeba elektrické energie se snižovaly se zvýšením teploty a zvýšením rychlosti deformace.

***Klíčová slova**: Laboratorní fyzikální modelování, děrování, bezešvé trubky, N80 uhlíková ocel, teplota, rychlost otáčení pracovních válců*

1. Introduction

N80 steel, as specified by API 5CT, is primarily used in the production of seamless pipes for oil and gas environments. The key properties of N80 steel include high strength, toughness, and resistance to corrosion caused by injected gases and fluids. The steel has broad chemical composition requirements and is available in two primary forms: normalized or hot-rolled (N80-1) and quenched and tempered (N80-Q) [1-3].

The first forming operation in the production of hot-rolled seamless tubes using the Mannesmann process is the punching of a full cylinder. This process, known as cross-rolling, is performed on a machine equipped with two eccentrically mounted double-cone working rolls and a supporting cylinder [4]. Additionally, a punch mandrel is placed in the gap between the rolls. The semi-finished product fed into the punching process can be a block, billet, or ingot with a full circular cross-section, or a semi-finished product with an axial bore. The punching process itself relies on the Mannesmann effect [5-7]. The punch mandrel helps smooth and expand the resulting cavity to the required dimensions. The outcome of the punching operation is a “perforated billet,” which serves as the semi-finished product to the next forming stage, known as rolling on a pilgrim’s stool [8-12]. Subsequent steps in the production process include calibration, heat treatment, finishing operations, and testing [13-17].

The subject of the present article is evaluation of the parameters involved in the physical modeling of punching a solid semi-finished product [18]. This is carried out using laboratory-scale punching equipment designed to simulate the production of seamless pipes, specifically a scale model of the Mannesmann rolling mill. Punching tests on the

laboratory rolling mill are conducted using solid samples or samples with a centrally pre-drilled circular cross-section.

Fig. 1 Laboratory rolling mill
Obr. 1 Laboratorní válcovací stolice

The rolling mill allows for precise adjustment of the axes of the working rolls in relation to the punching axis, achieved through both the cross angle and the forming angle. Additionally, the system provides the capability to adjust punching roller speeds within a range of 0 to 120 rpm. It is equipped with automated measurement systems to record various parameters, such as forces acting on the punching rollers, torques, forces on the mandrel bearing, roller speeds, electric current input, and others.

Fig. 1 presents a general view of the laboratory rolling mill from the entrance side. For sample heating, an electric resistance furnace is employed, which allows for the selection of different heating modes and the tracking of heating progress via a control computer. The furnace operates in an inert atmosphere to ensure controlled thermal conditions during testing.

This paper builds upon the authors' previous publications at MMV Company, which focused on the verification of punching process parameters [19], the impact of mandrel shape and positioning on punching technology [20], and the influence of process parameter settings on the dimensional characteristics of punched samples [21], among other related studies.

2. Experimental material and procedures

A series of 16 punching tests, varying heating temperature and rotational speeds of the working rolls, were conducted on a Mannesmann laboratory rolling mill. The heating temperatures ranged from 1240°C to 1300°C, in 20°C increments, and the roll speeds were set at 60 rpm and 120 rpm. To minimize process variability, each test was performed twice. The material used for the experiments was N80 carbon steel, as detailed in Tab. 1. The test samples, with a diameter of 70 mm and a length of 190 mm, were produced from a continuously cast billet with a diameter of 410 mm. The front circular side of each sample was machined with a conical bore to improve alignment with the punching mandrel. This conical feature helps reduce eccentricity during the punching process [22].

Tab. 1 Chemical composition of N80 steel
Tab. 1 Chemické složení oceli N80

Element	C	Mn	Si	P	S	Cu	Cr	V	Ni	Mo	Ti	Al	W	Nb	B	*N*	*Sn*	H	As	Co	*Sb*
[wt. %]	0.39	1.39	0.24	0.014	0.004	0.02	0.06	0.17	0.05	0.016	0.002	0.024	0.01	0.001	0.0006	0.008	*0.002*	*0.0001*	*0.002*	*0.003*	*0.001*

All punched samples were measured (Fig. 2), with specific attention to their minimum and maximum lengths, and diameters at the front, middle, and rear of the samples. Measurements were taken at two points around the circumference, separated by a 90° rotation, as outlined in Tab. 2. Based on these measurements, elongation and narrowing values were calculated for the front, middle, and rear sections of each punched sample (Tab. 3).

Additionally, the total punching time, torque values, forces acting on the work rolls, forces opposing the punching mandrel, and electrical current were recorded (Tab. 3). From these data, maximum and average values were calculated, along with the total current consumption for punching each individual sample (Tab. 4).

Fig. 2 Punched steel samples
Obr. 2 Vyděrované vzorky oceli

Hutnické listy č. 4-6/2024, roč. LXXVII
ISSN 0018-8069

Tab. 2 Experimental conditions and sample dimensions
Tab. 2 Podmínky experimentu a rozměry vzorků

Sample	RPM	Temp.	min. length	max. length	ϕfront1	ϕfront2	ϕmiddle1	ϕmiddle2	ϕback 1	ϕback 2
	[min^{-1}]	[°C]	[mm]							
1	120	1300	336	342	66.88	66.85	67.29	67.43	67.36	67.52
2	120	1300	338	340	66.92	67.13	67.46	67.56	67.36	67.23
3	60	1300	328	331	68.21	68.22	68.57	68.52	67.70	67.76
4	60	1300	340	343	66.74	66.81	67.70	67.76	67.77	67.76
5	120	1280	339	345	66.35	66.64	66.98	67.27	67.08	67.19
6	120	1280	347	350	66.09	66.23	67.29	67.33	66.94	66.92
7	60	1280	330	335	68.03	68.21	68.48	68.53	67.37	67.22
8	60	1280	330	333	68.30	68.28	68.88	68.86	67.21	67.56
9	120	1260	344	347	66.53	66.51	67.27	67.33	67.07	67.10
10	120	1260	330	334	67.62	67.91	68.26	68.35	67.75	67.86
11	60	1260	329	333	67.59	67.55	68.12	68.16	67.71	67.64
12	60	1260	333	335	67.92	68.02	67.88	67.82	67.45	67.47
13	120	1240	337	340	66.88	67.09	67.72	67.78	67.53	67.66
14	120	1240	340	343	66.70	66.79	67.67	67.84	67.59	67.52
15	60	1240	333	336	68.36	68.28	67.71	67.6	67.41	67.33
16	60	1240	315	320	69.80	70.12	70.37	70.12	68.17	68.11

Tab. 3 Total elongation, narrowing in different regions and total punching time
Tab. 3 Celkové prodloužení, úžení v různých oblastech vzorku a celková doba děrování

Sample	elongation	narrowing front	narrowing middle	narrowing back	time
	[-]	[%]			[s]
1	1.78	4.48	3.77	3.66	7.4
2	1.78	4.25	3.56	3.86	7.1
3	1.73	2.55	2.08	3.24	11.9
4	1.80	4.61	3.24	3.19	12
5	1.80	5.01	4.11	4.09	7.9
6	1.83	5.49	3.84	4.39	8.0
7	1.75	2.69	2.14	3.86	12.3
8	1.74	2.44	1.61	3.74	12.5
9	1.82	4.97	3.86	4.16	8.1
10	1.75	3.19	2.42	3.14	8.0
11	1.74	3.47	2.66	3.32	12.4
12	1.76	2.90	3.07	3.63	12.4
13	1.78	4.31	3.21	3.44	8.4
14	1.68	4.65	3.21	3.49	8.4
15	1.66	2.40	3.35	3.76	12.7
16	1.61	0.06	-0.35	2.66	12.8

Tab. 4 Experimental conditions and sample dimensions
Tab. 4 Podmínky experimentu a rozměry vzorků

Sample	max. torque	mean torque	max. axial force	mean axial force	max. press. force	mean press. force	max. current	mean current	elect. consumption
	[Nm]		[kN]				[A]		[As]
1	3948	2960	16.54	13.10	99.53	86.49	83.13	66.75	988
2	4181	2999	16.76	13.46	100.59	87.22	87.96	67.65	961
3	3962	2878	17.55	13.37	97.79	84.78	83.22	63.69	1516
4	4412	2962	18.48	14.07	100.16	85.81	91.72	65.58	1574
5	4473	3203	17.45	14.01	106.32	90.91	95.28	71.38	1128
6	4735	3356	18.64	15.33	109.00	91.9	98.39	74.20	1187
7	4190	3024	19.40	14.72	101,.90	87.3	87.60	66.76	1642
8	4159	3031	18.48	14.79	102.22	87.08	87.71	66.75	1669
9	4763	3417	19.35	15.86	111.06	93.08	101.56	74.97	1215
10	4601	3347	19.87	15.76	108.36	92.42	95.45	73.65	1178
11	4977	3286	21.12	16.58	110.03	90.93	102.13	72.03	1786
12	4520	3268	20.46	16.28	107.25	91.07	95.39	71.45	1772
13	4762	3494	20.59	16.72	112.16	95.46	102.59	76.77	1290
14	5023	3591	21.59	17.50	111.15	96.3	103.85	78.4	1317
15	4882	3448	21.45	16.82	109.01	92.61	100.41	74.34	1888
16	4830	3195	22.04	17.25	106.21	90.13	99.59	69.96	1791

The measured and calculated data were further analyzed and presented graphically in Fig. 3 to 11. Fig. 3 and 4 illustrate the temperature and rotational speed (rpm) dependence for the front, center, and rear sections of the punched samples. A clear trend is observed, where the rate of narrowing increases with both higher temperature and rpm. Fig. 5 shows the narrowing for each sample at the front, center, and rear; a negative value indicates material expansion. Figure 6 presents the effect of rpm and heating temperature on the overall elongation of the punched samples. A distinct increase in elongation is observed with higher temperature and rpm. At 120 rpm, the increase in elongation with temperature is less pronounced compared to tests conducted at 60 rpm.

The relationship between current consumption, rpm, and temperature is presented in Fig. 7, revealing a trend of reduced current consumption with increasing temperature and higher rpm. Fig. 8 and 9 illustrate the impact of rpm and temperature on the maximum and average forces acting on the work rolls. These figures show a gradual decrease in force with decreasing rpm and increasing temperature. Fig. 10 and 11 depict the effects of rpm and temperature on the maximum and average axial forces acting on the punch. In this case, the effect of rpm is minimal, with axial forces increasing slightly at higher rpm. However, as temperature increases, axial forces decrease.

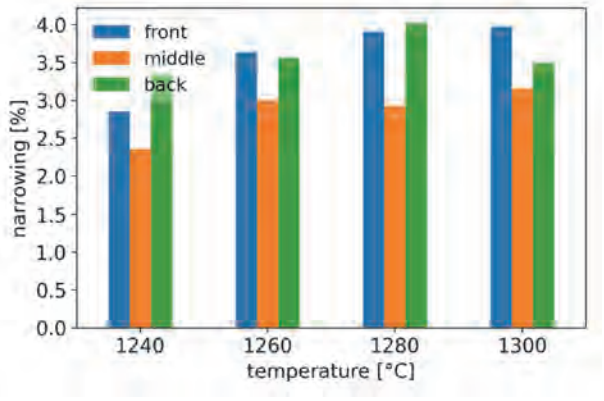

Fig. 3 Dependence of narrowing on temperature
Obr. 3 Závislost úžení na teplotě

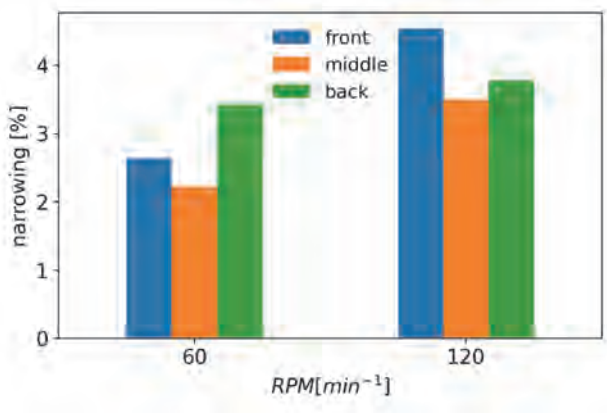

Fig. 4 Dependence of narrowing on work rolls speed
Obr. 4 Závislost úžení na rychlosti otáčení prac. válců

Hutnické listy č. 4-6/2024, roč. LXXVII
ISSN 0018-8069

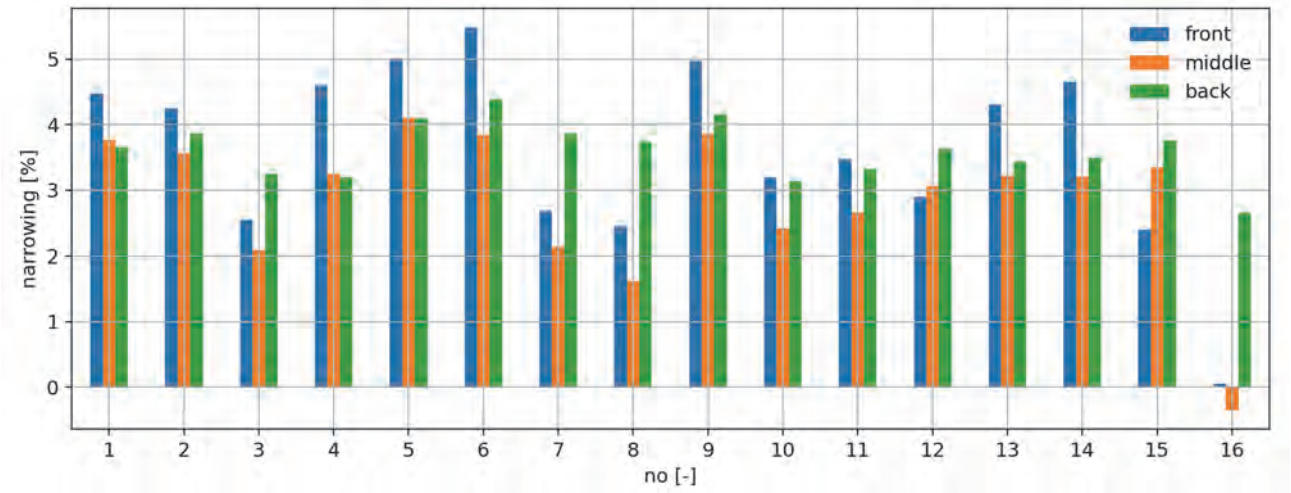

Fig. 5 Narrowing in different locations of all samples
Obr. 5 Úžení všech vzorků v různých oblastech

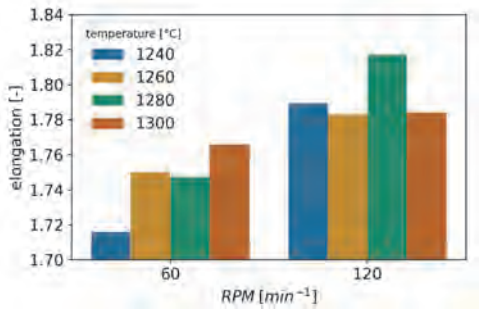

Fig. 6 Rolling elongation dependence on rolling speed for dif. temperatures
Obr. 6 Závislost prodloužení na rychlosti válcování pro různé teploty

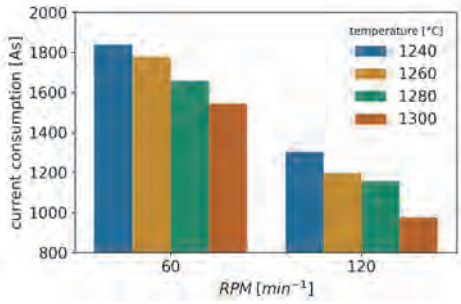

Fig. 7 Current consumption dependence on rolling speed for different temperatures
Obr. 7 Závislost elektrické spotřeby na válcovací rychlosti pro různé teploty

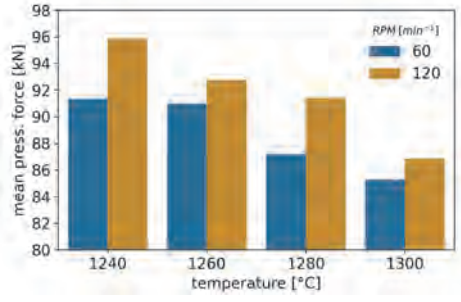

Fig. 8 Mean pressing forces dependence on temperature
Obr. 8 Závislost průměrných tlačných sil na teplotě

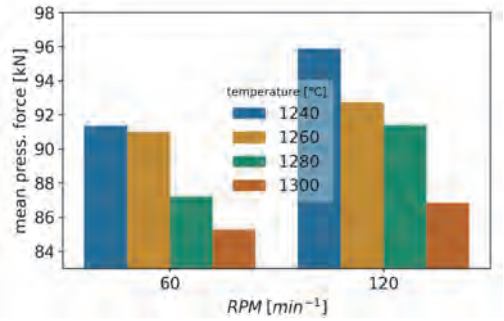

Fig. 9 Mean pressing forces dependence on working rolls speed
Obr. 9 Závislost průměrných tlačných sil na rychlosti válcování

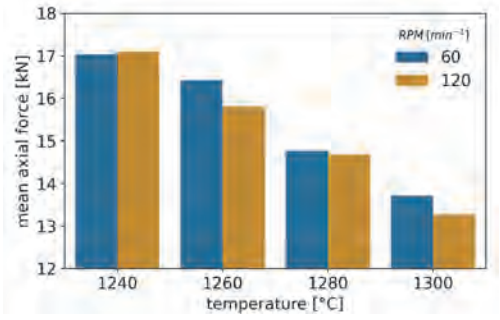

Fig. 10 Axial forces dependence on temperature
Obr. 10 Teplotní závislost axiálních sil

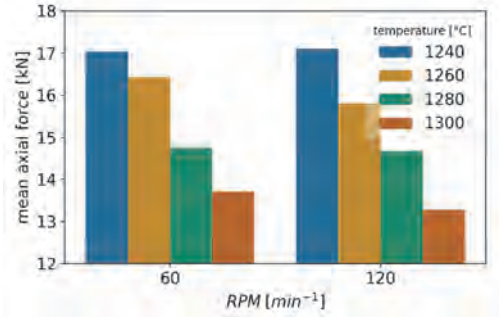

Fig. 11 Axial forces dependence on speed of working rolls
Obr. 11 Závislost axiálních sil na rychlosti válcování

3. Conclusion

This article presents the findings from punching experiments conducted on N80 carbon steel. The study focuses on identifying and mapping the trends of both measured and calculated parameters within the punching process, with heating temperature and rotational speed (rpm) selected as key variables. A significant observation from the tests at 120 rpm was a reduction in current consumption by approximately 40%, which was required for punching complete semi-finished products. The impact of heating temperature, however, was found to be less significant in comparison. As both temperature and rpm were increased, a corresponding rise in elongation and material narrowing was observed. Other notable trends include: an increase in elongation with higher rpm and temperature; a reduction in both average pressing force and axial force with increasing rpm; and a decrease in pressing and axial forces as temperature increased. These significant trends have been documented. The use of a laboratory rolling mill for physical simulations of the punching process has proven to be an optimal approach for investigating the interrelationships and trends among these various parameters. The findings will be expanded to include additional steel grades, allowing for a comparative analysis of final parameters across different materials. The primary objective of these tests is to simulate real-world industrial conditions, particularly in the production of seamless tubes, on a laboratory scale, with the ultimate goal of translating laboratory-based insights into practical industrial applications.

Acknowledgement

"This paper was created as a part of the drawing and use of institutional support for Long-term and conceptual development of a research organization in 2024, provided by the Ministry of Industry and Trade of the Czech Republic."

References

[1] XU, Tianhan, et al. Study on the static and dynamic fracture mechanism of different casing-drilling steel grades. *Materials characterization*, (2012), 67: 1-9.

[2] LOPEZ, D. A.; PEREZ, T. and SIMISON, S. N. The influence of microstructure and chemical composition of carbon and low alloy steels in CO2 corrosion. A state-of-the-art appraisal. *Materials & Design*, (2003), 24.8: 561-575.

[3] CHELGHAM, Fatiha, et al. Effects of Temperature on Microstructure and Corrosion behavior of API N80 Carbon Steel. *Asian Journal of Research in Chemistry*, (2021), 14.1: 61-66.

[4] WÓJCIK, Ł. and PATER, Z. Physical simulation of the Mannesmann effect in the rolling process. *Archives of Metallurgy and Materials* (2019), 1369-1375-1369-1375.

[5] SKRIPALENKO, M. M., et al. Mannesmann piercing of ingots by plugs of different shapes. *Materials Science and Technology*, (2016), 32.16: 1712-1720.

[6] SHU, Chang, et al. Influencing factors of void closure in skew-rolled steel balls based on the floating-pressure method. *Materials*, (2019), 12.9: 1391

[7] ZHENG, Zhenhua. Experimental Study on Cross Wedge Rolling of 21-4N Heat Resistant Steel. *Metals*, (2019), 9.1: 39. *Theoretical and Applied Fracture Mechanics*. 86 (2016), pp. 2-10.

[8] AN, Ning and HAI, Liu. Finite Element Analysis of Rolling Process for Pilger Mill. In: *Advanced Materials Research. Trans Tech Publications Ltd*, (2014). p. 1420-1423

[9] OSIKA, J. and LIBURA, W. Mathematical model of tube cold rolling in pilger mill. *Journal of Materials Processing Technology*, (1992), 34.1-4: 325-332

[10] POCIECHA, D., et al. Analysis of tube deformation process in a new pilger cold rolling process. *Archives of Civil and Mechanical Engineering*, (2014), 14.3: 376-382.

[11] FROLOV, Ya V.; MAMUZIĆ, I. and DANCHENKO, V. N. The heat conditions of the cold pilger rolling. *Metalurgija*, (2006), 45.3: 179-184.

[12] LEE, Sang-Kon and LEE, Kyung-Hun. Profile Design of the Grooved Die and Rolling Force Prediction in the Cold Pilger Rolling Process. *Applied Sciences*, (2021), 11.23: 11265.

[13] HU, Z. L., et al. Microstructure and mechanical properties of Al–Cu–Mg alloy tube fabricated by friction stir welding and tube spinning. *Scripta Materialia*, (2012), 66.7: 427-430.

[14] CHEN, Dong, et al. Online Cooling System and Improved Similar Self-adaptive Strategy for Hot-rolled Seamless Steel Tube. *ISIJ International*, (2021), ISIJINT2021-013.

[15] ZHANG, Zicheng, et al. Effect of heat treatment on microstructure and mechanical properties of TRIP seamless steel tube. *Materials Transactions*, (2012), 1203261608-1203261608.

[16] SEGURA, Alejandra, et al. Influence of anisotropy for the characterization of internal imperfections in pipes by ultrasonic non-destructive testing. NDT. net, (2009), 5: 2009.

[17] YAMANO, Masaaki, et al. Non-destructive Inspection Technique for Assuring the High-end Quality of Our Pipes and Tubes. *Nippon Steel & Metal Technical Report No. 397*, (2013), 125-130.

[18] UNUCKA, P. and NOGA, R. Physical modelling of seamless tubes producing. In *Metal 2013*, Brno: Tanger, 2013

[19] NOGA, R., UNUCKA, P. and VINDYŠ. M. Ověřování procesních parametrů děrování na laboratorní válcovací stolici. *Hutnické listy*, 67 (2014) 4, 36–39. ISSN 0018-8069.

[20] UNUCKA, P., NOGA, R., TUROŇ, R. and JURČA, R. Ověřování procesních parametrů děrování na laboratorní válcovací stolici. *Hutnické listy*, 67 (2014) 6, 51–54. ISSN 0018-8069.

[21] NOGA, R., JONŠTA, P., LIŠKA, M., TUROŇ, R. and JURČA, R., Vliv nastavení parametrů laboratorní děrovací stolice na rozměry vyděrovaného polotovaru oceli 4130. *Hutnické listy*, 72 (2019) 5, 29–34. ISSN 0018-8069.

[22] MURILLO-MARRODÁN, Alberto, et al. Analysis of wall thickness eccentricity in the rotary tube piercing process using a strain correlated FE model. *Metals*, (2020), 10.8: 1045.

[23] NOGA, R. and JONŠTA, P. Physical modeling of the seamless micro-alloyed steek tubes production depending on the different temperatures and rpm speeds of the working rolls. *METAL 2024*, Brno: Tanger, 2022.